

## Structural and Dynamic Properties of Solvated Hydroxide and Hydronium Ions in Water from *Ab Initio* Modeling

Renxi Liu,<sup>1,2</sup> Chunyi Zhang,<sup>3</sup> Xinyuan Liang,<sup>1,2</sup> Jianchuan Liu,<sup>1</sup> Xifan Wu,<sup>3,4</sup> and Mohan Chen<sup>1,2, a)</sup>

<sup>1)</sup>*HEDPS, CAPT, College of Engineering, Peking University, Beijing, 100871, China*

<sup>2)</sup>*Academy for Advanced Interdisciplinary Studies, Peking University, Beijing, 90871, China*

<sup>3)</sup>*Department of Physics, Temple University, Philadelphia, PA 19122, USA*

<sup>4)</sup>*Institute for Computational Molecular Science, Temple University, Philadelphia, PA 19122, USA*

(Dated: 12 October 2021)

Predicting the asymmetric structure and dynamics of solvated hydroxide and hydronium in water has been a challenging task from *ab initio* molecular dynamics (AIMD). The difficulty mainly comes from a lack of accurate and efficient exchange-correlation functional in elucidating the amphiphilic nature and the ubiquitous proton transfer behaviors of the two ions. By adopting the strongly-constrained and appropriately normed (SCAN) meta-GGA functional in AIMD simulations, we systematically examine the amphiphilic properties, the solvation structures, the electronic structures, and the dynamic properties of the two water ions. In particular, we compare these results to those predicted by the PBE0-TS functional, which is an accurate yet computationally more expensive exchange-correlation functional. We demonstrate that the general-purpose SCAN functional provides a reliable choice in describing the two water ions. Specifically, in the SCAN picture of water ions, the appearance of the fourth and fifth hydrogen bonds near hydroxide stabilizes the pot-like shape solvation structure and suppresses the structural diffusion, while the hydronium stably donates three hydrogen bonds to its neighbors. As a result, hydroxide prefers the stepwise proton transfer (PT) while hydronium prefers the concerted PT behavior. Consequently, hydroxide diffuses slower than hydronium in water, which is consistent with the experiments.

PACS numbers: 61.25.Em, 71.15.Pd, 82.30.Rs, 31.15.es

---

<sup>a)</sup>\*Corresponding author. Email:mohanchen@pku.edu.cn

## I. INTRODUCTION

Hydronium and hydroxide are two ubiquitous ions behind all acid-base reactions in water. A variety of chemical reactions in an aqueous environment are influenced by the existence of the two ions. Therefore, understanding the structure and dynamics of both ions is important for the studying of water and various related research areas.<sup>1</sup> In addition, the solvated hydronium  $\text{H}_3\text{O}^+(\text{aq})$  and hydroxide  $\text{OH}^-(\text{aq})$  ions in water exhibit intriguing properties. For example, as explained by the Grotthuss mechanism,<sup>2</sup> the diffusion of hydronium (hydroxide) ion in an aqueous environment can be viewed as an excessive proton (proton hole) that hops among water molecules through continuous breakage and formation of hydrogen bonds (HBs) in water. This so-called proton transfer (PT) process leads to abnormally high diffusivities of the two ions, which have important implications in a wide variety of biological, environmental and industrial processes<sup>3-5</sup>. However, the structural similarity of the two ions does not bring to similar diffusivity, rather, hydronium diffuses twice as fast as hydroxide.<sup>6-9</sup> In fact, the PT process occurs on a relatively short timescale of picoseconds and is largely influenced by the H-bond network in water. Until now, the microscopic origin of the PT event is not fully understood in experiments. Instead, *ab initio* molecular dynamics (AIMD) can access the timescale of PT events and therefore plays an important role in explaining the PT events<sup>10,11</sup>.

The prerequisite of simulating the above two ions in water is an accurate description of bulk water from AIMD. In the last few decades, AIMD simulations based on the density functional theory (DFT)<sup>12,13</sup> have been widely utilized to characterize bulk water because the accuracy and efficiency are reasonably balanced.<sup>14-19</sup> However, modelling of bulk water is non-trivial because several competing physical effects are present. Specifically, bulk water at ambient conditions is comprised of water molecules embedded within a continuously fluctuating H-bond network, which originates from a delicate balance among various physical interactions including covalent bonds, H-bonds, and van der Waals interactions.<sup>20-22</sup> Importantly, the balance between intra-molecular and inter-molecular interactions in liquid water largely depends on the choice of exchange-correlation (XC) functionals utilized in DFT. Early AIMD simulations of water<sup>23,24</sup> based on the LDA or GGA XC functionals predicted an over-structured H-bond network of water, resulting in sluggish and rigid water with a low density.<sup>20,25</sup> Later, adding van der Waals interactions upon GGA functionals has be-

come a common practice to yield a better description of structural and dynamic properties of water, as well as restoring the water density at ambient conditions.<sup>20-22,26-28</sup> On one hand, the van der Waals interactions increase the non-directional attraction forces between water molecules, which compensate for the underestimated water density.<sup>21</sup> On the other hand, the PBE0 hybrid functional<sup>29,30</sup> mitigates the self-interaction error and better accounts for the molecular polarizability in liquid water simulations,<sup>22</sup> resulting in weakened HBs between water molecules that are closer to experiments. The above two corrections draw the accuracy of simulating water towards experimental data.

Simulating  $\text{H}_3\text{O}^+(\text{aq})$  and  $\text{OH}^-(\text{aq})$  ions in water is more challenging than bulk water. Although AIMD simulations using different exchange-correlation functionals generally yielded similar structures and dynamics for solvated hydronium,<sup>14,16,31</sup> different GGA functionals such as PW91<sup>32</sup>, HCTC<sup>33</sup>, and BLYP<sup>15,19,34,35</sup> gave rise to dramatically different solvation structures and dynamics of solvated hydroxide. Therefore, the difficulty is particularly prominent in modeling hydroxide because it has more than one solvation structure. For example, the hydroxide ion described by PW91 favors a 3-fold coordination structure (tetrahedral structure), while those described by HCTH and BLYP favor a 4-fold coordination structure (hyper-coordination structure).<sup>15</sup> Previous studies proposed that the hyper-coordination structure strongly suppresses the PT events.<sup>15,36</sup> As a result, the two distinct H-bond structures lead to distinct diffusivities of the hydroxide ion. Although the BLYP functional predicts reasonable diffusion coefficients of hydroxide, it substantially underestimates the density of liquid water ( $0.75 \text{ g/cm}^3$ ),<sup>26</sup> implying that the BLYP functional is not adequate to describe the sophisticated H-bond network of liquid water. Importantly, the BLYP functional predicted that both hydronium and hydroxide ions prefer to experience bursts of PT events than single PT events within a timescale of water wire compression.<sup>17,18</sup> These ubiquitous concerted PT behaviors of the two ions are highly correlated in time, which adds a new twist to the already sophisticated story but does not provide enough evidence to explain the slower diffusivity of  $\text{OH}^-(\text{aq})$  than that of  $\text{H}_3\text{O}^+(\text{aq})$ .

The concerted PT picture is updated via considering both exact exchange and van der Waals interactions in AIMD simulations.<sup>16</sup> By utilizing the hybrid functional PBE0<sup>29</sup> with the self-consistent Tkatchenko-Scheffler (TS) functional in AIMD simulations,<sup>22,37</sup> the so-called PBE0-TS exchange-correlation functional mitigates the spurious self-interaction and includes both intermediate- and long-range van der Waals interactions. This leads to a better

description of the H-bond network of liquid water, where structural and dynamic properties of  $\text{OH}^-(\text{aq})$  and  $\text{H}_3\text{O}^+(\text{aq})$  are substantially improved towards the experimental data. For example, while previous AIMD simulations utilizing GGA functionals suggested that the hydroxide has a planar solvation structure,<sup>15,38</sup> the PBE0-TS predicted a pot-like solvation structure of hydroxide that agrees with the picture from neutron scattering data.<sup>16,39</sup> In addition, unlike BLYP, the PBE0-TS functional largely stabilized the 4-fold solvation structure of  $\text{OH}^-(\text{aq})$ , which inhibits the concerted PT behaviors of hydroxide. Instead, the solvated hydroxide ion described by PBE0-TS exhibits a stepwise motion. Meanwhile,  $\text{H}_3\text{O}^+(\text{aq})$  still preserves the concerted PT behavior within the description of PBE0-TS. Consequently, PBE0-TS predicts a slower diffusivity of hydroxide than hydronium,<sup>16</sup> which agrees well with the experiments.<sup>7-9</sup>

Unfortunately, despite the apparent merits of utilizing linear-scaling PBE0-TS<sup>40</sup> in studying liquid water and ions, the prefactor of the linear-scaling method is still large and the computational costs are extremely high. In this regard, the community awaits an accurate yet efficient XC functional that can be utilized to study not only liquid water but also  $\text{OH}^-(\text{aq})$  and  $\text{H}_3\text{O}^+(\text{aq})$  ions. Notably, the recently proposed SCAN functional,<sup>41</sup> fulfilling all 17 known exact requirements on the semilocal XC functional, can achieve similar accuracy as PBE0-TS does in describing the structural and dynamic properties of liquid water at ambient conditions, as well as the water density.<sup>21</sup> In particular, the computational cost of SCAN is comparable to GGA functionals but about an order of magnitude smaller than the PBE0-TS functional for studying condensed phases.<sup>42</sup> Compared to GGA functionals, SCAN predicts stronger covalent bonds within water molecules and less negatively charged local environment around the oxygen atom. As a result, the directional HBs are weakened. In addition, the intermediate-ranged van der Waals interaction in SCAN provides attractive forces among water molecules, which leads to the movements of the second-shell water molecules towards the non-H-bonded interstitial area, creating a more disordered and denser structure on the intermediate range. The above changes provided by SCAN results in a weakened H-bond network of liquid water that is closer to the experimental data.<sup>43,44</sup> As a result, SCAN provides better structural and dynamic properties of liquid water than PBE.<sup>21</sup> This is considered to be the main reason why SCAN, rather than PBE and other GGA functionals, predicts the correct quantitative relation between densities of water and ice under ambient conditions.<sup>21</sup> Furthermore, SCAN also exhibits high precision in modeling

water clusters, gas and ice phase water, which outperforms GGA functionals.<sup>45–49</sup>

Nevertheless, to the best of our knowledge, the effects of the SCAN functional in describing the structure and dynamics of water ions have not been thoroughly explored yet. In this work, we have performed AIMD simulations of  $\text{OH}^-$ (aq) and  $\text{H}_3\text{O}^+$ (aq) ions using the SCAN exchange-correlation functional. Detailed analysis was performed on these AIMD trajectories to evaluate the amphiphilic properties, the solvation structures, the electronic structures, and the dynamic properties. In particular, the SCAN results are systematically compared to the PBE0-TS results,<sup>16</sup> which serve as a valid benchmark to evaluate the performances of SCAN for  $\text{OH}^-$ (aq) and  $\text{H}_3\text{O}^+$ (aq) ions. The paper is organized as follows, Section II introduces the computational details. The AIMD results are shown and discussed in Section III, and the concluding remarks are presented in Section IV.

## II. COMPUTATIONAL DETAILS

We have performed AIMD simulations by using the Car-Parrinello molecular dynamics method<sup>50</sup> implemented in the Quantum ESPRESSO package.<sup>51</sup> We used 63 water molecules and a hydroxide or hydronium ion in a periodic cubic cell with a length of 12.4447 Å. A kinetic energy cutoff of 85 Ry was adopted. We used the meta-GGA exchange-correlation functional in the form of SCAN<sup>41</sup> and the Hamann-Schlüter-Chiang-Vanderbilt pseudopotentials generated with the PBE functional.<sup>52</sup> For the AIMD simulations, we adopted the Nosé-Hoover chain thermostats with a chain length of 4 for each ion to control the temperature of 330 K in the NVT ensemble.<sup>53–55</sup> The mass of hydrogen atom was set to 2.0141 (mass of deuterium). A fictitious electron mass of 100 a.u. was used along with a mass cut-off of 25 a.u. The AIMD trajectory lengths were 124.4 and 176.9 ps for the hydroxide and hydronium simulations, respectively. A time step of 2.0 a.u was adopted. AIMD results utilizing the PBE0-TS XC functional referenced from literature<sup>16</sup> were also shown, which serve as a baseline to elucidate the effects of the SCAN functional in predicting properties of hydronium and hydroxide in an aqueous environment. A standard hydrogen bond criterion was adopted<sup>10</sup>. Specifically, two neighboring water molecules are defined to be H-bonded when the O-O distance is less than 3.5 Å, the inter-water O-H distance is less than 1.24 Å, and the O-O-H angle is less than 30°.

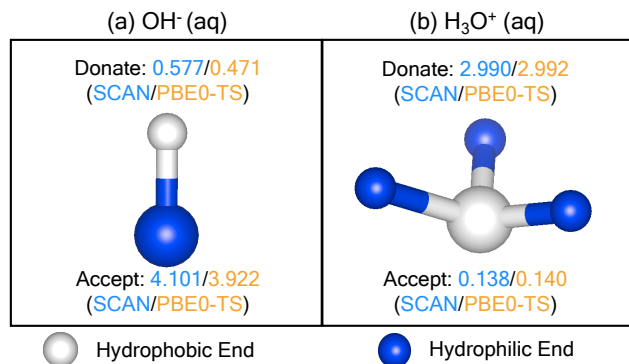


FIG. 1. Hydrophobic (gray) and hydrophilic (blue) ends in solvated (a) OH<sup>-</sup>(aq) and (b) H<sub>3</sub>O<sup>+</sup>(aq) ions. Average number of accepted and donated hydrogen-bonds (HBs) for both ions is listed. Two exchange-correlation functionals, i.e., SCAN and PBE0-TS, are used.

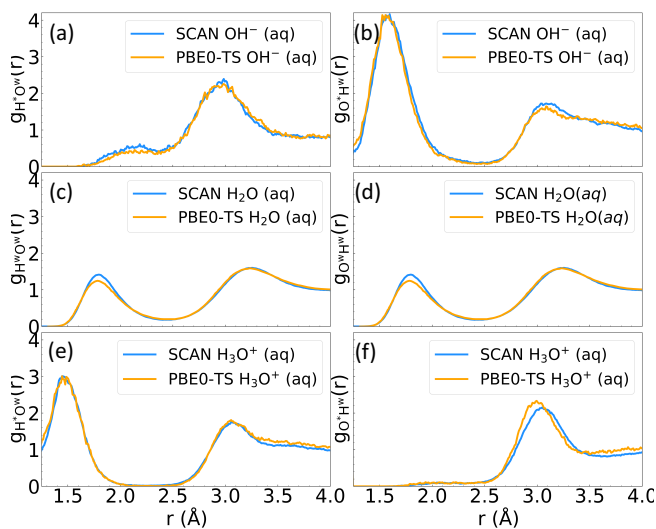


FIG. 2. Radial distribution functions  $g(r)$  as extracted from SCAN (blue) and PBE0-TS (orange) trajectories. Superscripts \* and w depict atoms in ions and water molecules, respectively. (a), (c) and (e) respectively show the distribution of O atoms around H atoms in the OH<sup>-</sup>(aq), H<sub>2</sub>O and H<sub>3</sub>O<sup>+</sup>(aq) molecules, while those in (b), (d) and (f) display the distribution of H atoms around O atom in the OH<sup>-</sup>(aq), H<sub>2</sub>O and H<sub>3</sub>O<sup>+</sup>(aq) molecules, respectively.

### III. RESULTS AND DISCUSSION

#### A. Amphiphilic Properties

Both  $\text{OH}^-(\text{aq})$  and  $\text{H}_3\text{O}^+(\text{aq})$  ions are amphiphilic in nature as compared to the water molecules. Fig. 1 shows the hydrophobicity and hydrophilicity of different ends in both ions, as well as the number of HBs for each end. The oxygen site of  $\text{OH}^-(\text{aq})$  is hydrophilic and the hydrogen site is hydrophobic; on the contrary, the oxygen site of  $\text{H}_3\text{O}^+(\text{aq})$  is hydrophobic while the hydrogen site is hydrophilic. Fig. 2 illustrates the radial distribution functions  $g(\mathbf{r})$  of solvated hydroxide and hydronium ions, as well as those of the ambient liquid water from AIMD simulations using both SCAN and PBE0-TS XC functionals. Note that the superscripts \* and w denote an atom from an ion and a water molecule, respectively. On one hand, the two ions are hydrophobic, as respectively illustrated in Figs. 2 (a) and (f),  $g_{\text{H}^*\text{O}^w}(\mathbf{r})$  of hydroxide and  $g_{\text{O}^*\text{H}^w}(\mathbf{r})$  of hydronium both exhibit the reduced HBs of the first solvation shell as compared to ambient liquid water. Specifically, the hydroxide (hydronium) ion shows a strong repulsion against water molecules on its hydrogen (oxygen) site by largely reducing the donated (accepted) HBs with neighboring atoms. On the other hand, the two ions are hydrophilic, which can be seen in Figs. 2(b) and (e) as the first peak of  $g(\mathbf{r})$  shifts to the left when compared to its counterpart in pure liquid water. In detail, for the first high peak of  $g_{\text{O}^*\text{H}^w}(\mathbf{r})$  shown in Fig. 2(b), the oxygen site of the hydroxide ion attracts multiple neighboring water molecules via forming HBs, while the first high peak of  $g_{\text{H}^*\text{O}^w}(\mathbf{r})$  shown in Fig. 2(e) implies that the hydrogen sites of the hydronium stably donate three protons to neighboring water molecules and form HBs. As will be explained below, the amphiphilic nature of the two ions leads to their unique structural and dynamic properties.

Unlike some GGA functionals that yield qualitatively different radial distribution functions for hydroxide,<sup>15</sup> the SCAN functional yields a  $g(\mathbf{r})$  similar to that predicted by PBE0-TS, as shown in Fig. 2. Regarding the computational costs, SCAN takes the advantage of being much more efficient than the hybrid functional.<sup>21</sup> Therefore, it is valuable to compare properties of hydroxide and hydronium in detail as obtained from the two functionals and we have the following findings. First, the hydrophobic sites of the two ions are investigated. We observe a less hydrophobic end in hydroxide (hydrogen site) as compared to that in hydronium (oxygen site), because the first and the second peaks of  $g_{\text{H}^*\text{O}^w}(\mathbf{r})$  for hydroxide

in Fig. 2(a) are considerably higher than those in the  $g_{O^*H^w}(r)$  for hydronium shown in Fig. 2(f), suggesting more water molecules locate around the hydrogen site of hydroxide than the oxygen site of hydronium. When comparing the results from SCAN to those from PBE0-TS, the hydrophobic site of hydroxide, i.e., the hydrogen of hydroxide, becomes less hydrophobic by donating slightly more HBs to its neighbors. This is evidenced as SCAN yields a higher first peak of  $g_{H^*O^w}(r)$  than PBE0-TS in Fig. 2(a). The result is also consistent with the HB data shown in Fig. 1, where the averaged number of donating HBs in hydroxide is 0.577 and 0.471 from SCAN and PBE0-TS, respectively. On the contrary, the hydrophobic site of hydronium, i.e., the oxygen site, becomes more hydrophobic by adopting the SCAN functional, which is evidenced by a lower first peak of  $g_{O^*H^w}(r)$  located around 3 Å in Fig. 2(f). Moreover, the peak locates further away from the central atom than the one from PBE0-TS, suggesting that it would be more difficult for hydronium to accept HBs in SCAN (0.138) than in PBE0-TS (0.140), as listed in Fig. 1.

Second, we focus on the hydrophilic sites of the two ions, where multiple HBs form between the ion and water molecules. Notably, the symmetric picture for the twin topological defects, i.e., hydroxide and hydronium ions, is invalid from both XC functionals if we inspect the coordination number of the two ions. Specifically, the height of the first peak at the hydrophilic end of hydroxide (Fig. 2(b)) is higher than that of hydronium (Fig. 2(e)), indicating a larger coordination number. For example, according to the HB analysis of the SCAN trajectory in Fig. 1, hydroxide accepts 4.101 HBs on average, which is larger than hydronium that donates 2.990 H-bonds. Meanwhile, the oxygen site of hydroxide described by PBE0-TS donates 3.922 HBs, which exhibits less hydrophilic property as compared to the one by SCAN. Furthermore, we observe more non-H-bonded water molecules in the second shell of hydroxide from the SCAN functional, which can be seen by a higher second peak of  $g_{O^*H^w}(r)$  in Fig. 2(b). The above structural features of hydroxide imply that SCAN gathers more H-bonded water molecules around both ends of hydroxide than PBE0-TS.

The amphiphilic nature of the two ions can be further analyzed by the HB statistics of the hydroxide and hydronium ions. As found by previous studies<sup>15,16</sup>, the hydronium cation stably donates three HBs but the hydroxide ion has two H-bonded solvation structures, i.e., a nearly tetrahedral structure with three acceptor HBs and a hyper-coordinated structure with four or more acceptor HBs. While the PBE functional predicts more tetrahedral-like structures of hydroxide, the inclusion of van der Waals interactions and self-interaction

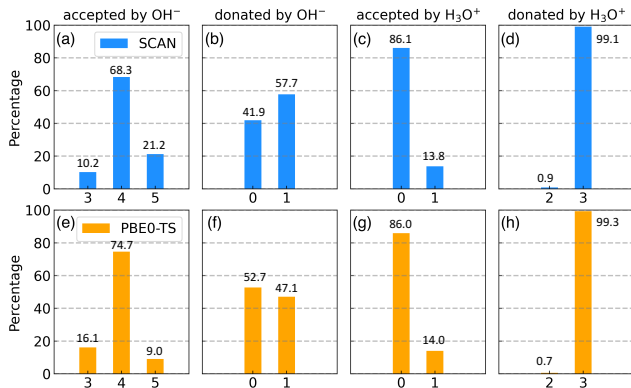


FIG. 3. Percentages of H-bonds for  $\text{OH}^-(\text{aq})$  and  $\text{H}_3\text{O}^+(\text{aq})$  ions. The first row (a-d) presents results from the SCAN functional (blue), while the second row (e-h) displays those from the PBE0-TS functional (orange).

correction helps to soften and stabilize the hypercoordination of hydroxide.<sup>16</sup> Importantly, both SCAN and PBE0-TS functionals include the van der Waals interactions and predict a majority of hydroxide ions that accept four or more HBs to form the so-called hyper-coordinated structure, which are shown in Figs. 3(a) and (e). For instance, 68.3% and 74.7% of hydroxide ions with four accepted HBs are found in the SCAN and PBE0-TS trajectories, respectively. Interestingly, the SCAN functional predicts substantially more hydroxide ions that accept 5 HBs (21.2%) than the PBE0-TS functional (9.0%). Additionally, SCAN and PBE0-TS give rise to 10.2% and 16.1% of hydroxide ions that accept 3 HBs. The above analysis suggests that although both hydroxide ions predicted by SCAN and PBE0-TS tend to form the stable hyper-coordinated solvation structure, the distributions of formed HBs still exhibit some deviations.

## B. Solvation Structures

Early AIMD simulations predicted the solvation structure of the hydroxide to be planar-like.<sup>15</sup> However, a pot-like solvation structure of hydroxide was suggested by the neutron diffraction experiment coupled with empirical potential structure refinement.<sup>39</sup> Figs. 4(a) and (b) illustrate the spatial distributions of the first solvation shell of hydroxide as obtained from the SCAN and PBE0-TS functionals, respectively. From the figure, we can see that the usage of both functionals leads to a pot-like shape of the solvation structure, which is

close to the experimental data.<sup>39</sup>

In comparison with the pot-like shape of the solvation structure from PBE0-TS, SCAN also provides a pot-like shape of the solvation structure but with a thinner bottom, which is closely related to the number of accepted H-bonds. As previously discussed, SCAN yields a larger portion of hydroxide ions which accept 5 HBs as compared to PBE0-TS. In this regard, we examine the solvation structure features of hydroxide with different coordination numbers as described by the two methods, in order to clarify how different XC functionals affect the solvation structure in detail. Figs. 4(a) and (b) plot the solvation structures of hydroxide in terms of accepting 4 (cyan) or 5 (grey) HBs in liquid water. For both functionals, we find that the pot-like solvation structure with 5 HBs occupies a larger volume as compared to the 4 HBs counterparts, especially on the top and bottom areas of the pot-like solvation structure. This indicates that the accepted fifth oxygen atom locates further away from the hydroxide ion. Interestingly, when accepting its fifth H-bond, the hydroxide described by SCAN tends to locate the HB at the bottom of the ‘pot’, while PBE0-TS tends to place the HB on the top. It is worth mentioning that while the excessive HB does not influence the distribution of donated HB in the SCAN trajectory, it substantially affects the distribution of donated HB in the PBE0-TS trajectory, as Fig. 4(b) shows that the lid of the pot becomes thinner when the hydroxide accepts 5 HBs as compared to 4 HBs.

We further compare the planarity order parameter  $p(r)$  to understand the local solvation structure of hydroxide that accepts 4 HBs. The parameter  $p(r)$  is defined as the distance from the fourth accepted oxygen atom of hydroxide to the plane formed by the other three oxygen atoms.<sup>16</sup> Fig. 5 illustrates the  $p(r)$  of hydroxide from the SCAN and PBE0-TS trajectories. The two trajectories lead to substantial differences in  $p(r)$ . For example,  $p(r)$  of SCAN exhibits a notable distribution from zero to around 2.0 Å, while  $p(r)$  of PBE0-TS owns a peak located at a larger planarity. Essentially, the results suggest that the hydroxide ion described by SCAN gives rise to a more planar distribution of accepted O atoms, while the PBE0-TS softens the directional HB strength by mitigating self-interaction error and forms a pot-like solvation structure. The analysis is in accordance with the above comparison made between the cyan isosurfaces in Figs. 4(a) and (b). Notably, the pot-like solvation structure by SCAN relies more on the relatively abundant 5-coordinated HB structure, which yields a solvation structure with a thinner bottom as compared to PBE0-TS. In regard to the relationship between solvation structure and diffusion, a more planar geometry of the

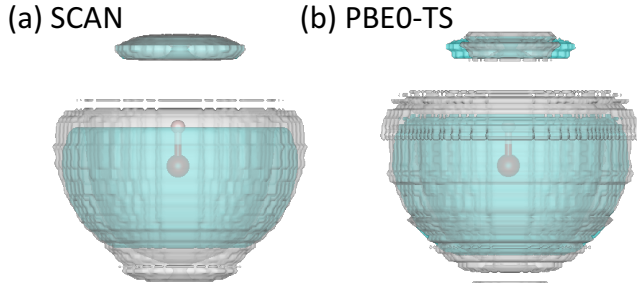


FIG. 4. Solvation structures of  $\text{OH}^-(\text{aq})$  in ambient liquid water as computed from AIMD trajectories utilizing the (a) SCAN and (b) PBE0-TS functionals, respectively. The cyan and grey isosurfaces represent the solvation structures of  $\text{OH}^-(\text{aq})$  when it accepts 4 and 5 HBs, respectively. The red and white atoms depict the oxygen and hydrogen atoms, respectively.

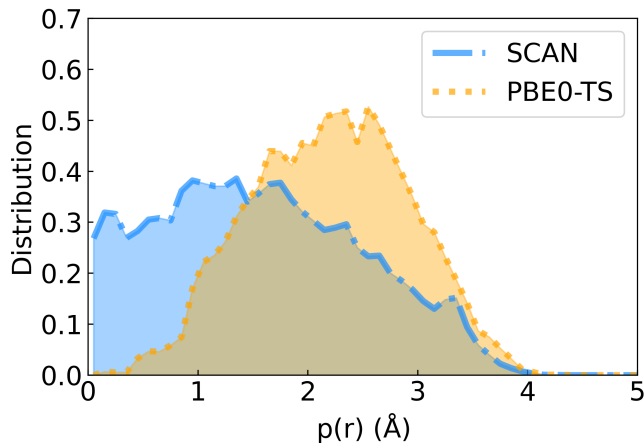


FIG. 5. Distributions of the planarity order parameter calculated with SCAN and PBE0-TS trajectories are shown. The planarity order parameter  $p(r)$  is defined as the distance from an oxygen atom to the plane formed by the other three oxygen atoms in water molecules.

solvation structure of hydroxide deviates more from a tetrahedral HB network of water than PBE0-TS, resulting in a more stable asleep mode of hydroxide.

### C. Electronic Structures

The hydrogen bond is largely comprised of electrostatic attractions, which is determined by the electronic structures from DFT calculations. In AIMD, the local electronic structure associated with chemical bonds can be conveniently described by the maximally localized Wannier functions (MLWFs), which are obtained by unitary transformation of the DFT

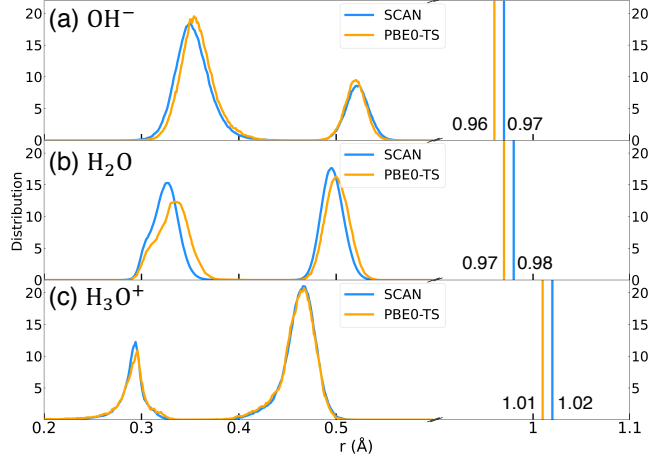


FIG. 6. (a), (b), and (c) respectively illustrate the distributions between the oxygen atoms of  $\text{OH}^-$ (aq),  $\text{H}_2\text{O}$ , and  $\text{H}_3\text{O}^+$ (aq) molecules and the centers of the corresponding maximally localized Wannier functions. Blue and orange lines represent the data extracted from the SCAN and PBE0-TS trajectories, respectively. Vertical lines represent the average lengths of the O-H covalent bond.

eigenfunctions. To be specific, in a molecular dynamics trajectory, the information for the electronic environment for water molecules can be deduced from the statistical analysis of the MLWF centers. Figs. 6(a), (b), and (c) show the distributions of centers of MLWFs representing electronic information in  $\text{OH}^-$ (aq),  $\text{H}_2\text{O}$ , and  $\text{H}_3\text{O}^+$ (aq) molecules in ambient liquid water, respectively. The four Wannier function centers surrounding a water molecule or water ion are divided into two peaks according to their distances to the central oxygen atom. The peak located closer to the O atom represents the lone pairs of electrons while the peak further from the O atom represents the bonding pairs of electrons constituting covalent bonds.

The positions of the lone pairs and bonding pairs of electrons determine the amphiphilic nature of molecules. Taking the SCAN trajectories as an example, Figs. 6(a) and (b) illustrate that the length of covalent bond in hydroxide and ambient liquid water, i.e., the distance between the oxygen and the proton, is 0.97 and 0.98 Å, respectively. Meanwhile, the distance between the oxygen atom and the covalent bonding pairs in hydroxide and in liquid water is 0.52 and 0.49 Å, respectively. Therefore, the distance between the proton and the electron bonding pairs is smaller in hydroxide (0.45 Å) than in liquid water (0.49 Å), leading to a less positively charged environment of hydrogen in hydroxide. The above explains the origin of the hydrophobic site in the hydroxide anion, where the formation of

HBs is hindered due to the weak electrostatic attraction force. On the other hand, the lone pair of hydroxide locates further away from the oxygen atom (0.35 Å) than the lone pairs of liquid water molecules (0.33 Å), which brings the hydroxide ion a more negatively charged local environment around its oxygen site. Consequently, this leads to the hydrophilic property of hydroxide anion, where acceptance of HBs becomes easier than water molecules. In stark contrast, the electron bonding pairs of hydronium cation stay further away from the protons, creating a more positively charged (hydrophilic) environment to stably form three HBs, as illustrated in Fig. 6(c); the oxygen site of hydronium stays closer to the lone pair, leading to a less negatively charged environment that exhibits hydrophobic properties.

Now we compare the detailed electronic structure differences of the two ions from SCAN and PBE0-TS. First, as shown in Figs. 6(a), (b), and (c), a larger distance between oxygen and proton (the length of O-H covalent bond) suggests that oxygen binds more loosely with the proton, and SCAN is known to strengthen the covalent bonds as compared to PBE<sup>21</sup>; here we find PBE0-TS yields protons that locate closer to the oxygen atom, implying a stronger covalent bond as compared to SCAN. Besides, for the pure water described by the SCAN functional, both lone pairs and bonding pairs of ambient liquid water molecules shown in Fig. 6(b) shift closer to the oxygen atom. This indicates that SCAN provides a less negatively charged environment on the oxygen site and a more positively charged environment on the proton side for pure liquid water. In other words, the oxygen and proton sites of water molecules respectively become more hydrophobic and more hydrophilic in the SCAN trajectory than in the PBE0-TS counterpart. The two competing effects lead to a more pronounced first peak of radial distribution functions as observed in Figs. 2(c) and (d), which implies that SCAN provides a more strengthened HB at a short-range scale when compared to PBE0-TS.

Second, for the hydroxide anion illustrated in Fig. 6(a), the location of the electron bonding pair is slightly further away from the central oxygen, as predicted by SCAN and compared to that from PBE0-TS. Nevertheless, the proton locates further away from the bonding pair as described by SCAN, suggesting a stronger hydrophilicity of the originally hydrophobic proton site in hydroxide. This leads to an increased number of donated HBs from PBE0-TS (0.471) to SCAN (0.577), as abovementioned. For the other site of the hydroxide anion (oxygen), when comparing the results from SCAN to those from PBE0-TS, the former provides a shortened distance between the lone pair and the oxygen atom,

creating a more hydrophobic oxygen site of hydroxide. However, a competing effect arises due to the usage of SCAN, i.e., the protons of water molecules become more hydrophilic. As a result, the oxygen site of hydroxide in the SCAN trajectory accepts more HBs (4.101) than that of PBE0-TS (3.922), as listed in Fig. 1. The above differences that exist in the electronic structures of hydroxide anion lead to the deviation of the solvation shell structure shown in Fig. 4.

Third, by analyzing the distribution of MLWF centers of hydronium cation from the SCAN and PBE0-TS trajectories shown in Fig. 6(c), we observe that SCAN provides a more hydrophilic environment for the proton sites of hydronium because the distance between the bonding pair and the protons is larger. In addition, the protons of hydronium interact with the more hydrophobic oxygen of water molecules. As a result, hydronium from both trajectories donate three stable HBs, suggesting that SCAN and PBE0-TS yield similar short-ranged structure information for the proton sites of hydronium. On the other hand, for the oxygen site of hydronium, the lone pair from SCAN locates slightly closer to the oxygen atom as compared to the one from PBE0-TS, which creates a slightly more hydrophobic environment for hydronium. In this regard, it is consistent that hydronium cation accepts 0.138 HBs from SCAN, which is marginally smaller than the 0.140 HBs from PBE0-TS, as listed in Fig. 1.

In conclusion, for water ions including the hydronium and hydroxide ions, as well as the water molecules, we analyze their electronic structures via the distribution of MLWF centers. In general, compared to the results from PBE0-TS, we find that the SCAN functional yields a closer distance between the lone pairs and the oxygen atom, and a larger distance between the bonding pairs and protons. In addition, the hydrophilic and hydrophobic nature of the two ions are affected by considering the delicate interactions between the ions and neighboring water molecules. Consequently, when comparing the SCAN results with the PBE0-TS results, the hydroxide anion from SCAN becomes more hydrophilic, while the hydronium cation from SCAN becomes slightly more hydrophobic.

#### D. Dynamic Properties

Diffusion of solvated  $\text{OH}^-(\text{aq})$  and  $\text{H}_3\text{O}^+(\text{aq})$  ions is contributed by two parts, including the structural diffusion via PT and the hydrodynamics (the Stokes diffusion) processes. The

ubiquitous fast diffusion of water ions origins from the PT process, as explained by the Grotthuss mechanism.<sup>2</sup> With the advances of AIMD techniques and computational powers, PT events that occur with a time scale of picoseconds are accessible via AIMD simulations. The remaining key problem, however, is the frequency of PT events that determines the diffusion coefficients of the two ions. While most XC functionals yield a similar mechanism for the diffusion of the  $\text{H}_3\text{O}^+(\text{aq})$  cation, the diffusion mechanism of the  $\text{OH}^-(\text{aq})$  anion remains inconclusive or even contradictory.<sup>15</sup> This is mainly due to the fact that different XC functionals yield different proportions of the tetrahedral and hyper-coordinated solvation structures of hydroxide.<sup>15</sup> Recent works have pointed out that the PT events are highly correlated in time as bursts of PT events within a short time was observed for both ions;<sup>18</sup> however, the picture is later revised to be valid only for hydronium, while the PT events of hydroxide prefers to be stepwise.<sup>16</sup> The reason, as explained by AIMD simulations with the PBE0-TS functional in Ref. 16, is the increased proportion of the asleep mode (the hyper-coordinate solvation structure) that hinders the concerted PT of the hydroxide anion.

Essentially, a conceptually correct picture of the structural diffusion of  $\text{OH}^-(\text{aq})$  and  $\text{H}_3\text{O}^+(\text{aq})$  ions relies on a precise description of the HB network of water, as well as the solvation structures of water ions. Although the issues are well addressed by the PBE0-TS functional,<sup>16</sup> the computational cost is extremely high. As abovementioned, the number of formed HBs between molecules stands as a major indicator of hydrophobicity and hydrophilicity. Generally dictated by electronic structures, the HB network of water and ions is mainly determined by the used XC functional.<sup>15,19–28,32,33</sup> Therefore, we validate the performance of the SCAN XC functional in providing the frequency of the PT events and the relevant dynamic properties for the two ions, and compare them to the PBE0-TS results.

In order to quantitatively describe the frequency of concerted PT events in these AIMD trajectories, we categorize the PT events according to the number of transfer events during one burst, as done in Ref. 16.<sup>?</sup> Figs. 7(a) and (c) display statistics of the concerted PT events for hydroxide by using the SCAN and PBE0-TS functionals, respectively. We find that the two functionals yield the same conclusion that PT events in the hydroxide system are dominated by both single and double jumps, while triple- and quadruple-jumps are relatively rare. In stark contrast, as illustrated in Figs. 7(b) and (d), where both functionals yield the same conclusion that the concerted PT events for hydronium is dominated by the double jumps, the frequency of which is substantially larger than the counterpart in

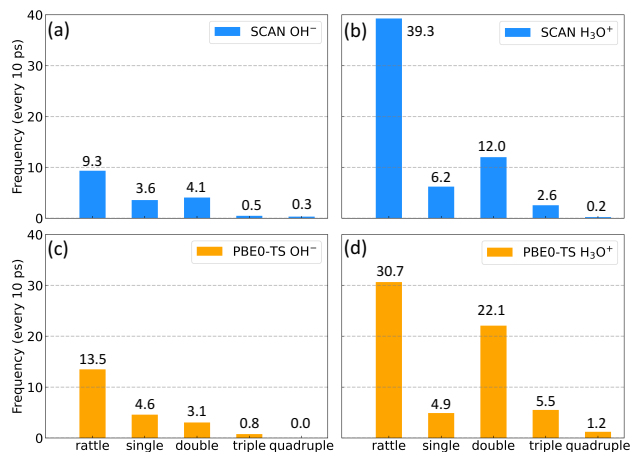


FIG. 7. Proton transfer frequencies of different proton transfer types are presented here. Detailed definition of these proton transfer types can be found in the text. (a-d) respectively represents OH<sup>-</sup>(aq), H<sub>3</sub>O<sup>+</sup>(aq) predicted by SCAN and OH<sup>-</sup>(aq), H<sub>3</sub>O<sup>+</sup>(aq) for PBE0-TS.

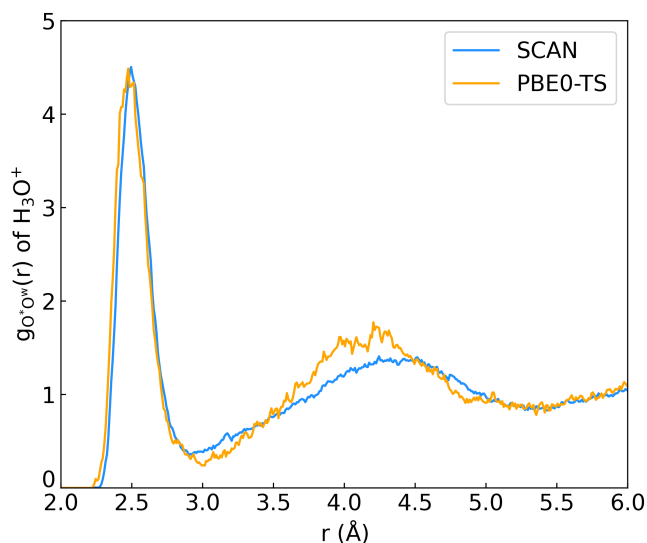


FIG. 8. Radial distribution functions involving O atoms in H<sub>3</sub>O<sup>+</sup> (O<sup>\*</sup>) and O atoms from neighboring water molecules (O<sup>W</sup>). Two trajectories involving SCAN and PBE0-TS exchange-correlation functionals are used.

hydroxide. For instance, the frequency of double jumps from SCAN (PBE0-TS) is 12.0 (22.1) times per 10 ps for hydronium, much larger than the value of 4.1 (3.1) for hydroxide. In addition, the triple- and quadruple-jumps are relatively rare in hydronium. Interestingly, the rattling event is defined as one atom jumps to its neighboring molecule and then returns

to the original molecule within 0.5 ps.<sup>16</sup> Apparently, hydronium undergoes more rattling events than hydroxide, which could be attributed to the fast alternate between the Zundel ( $\text{H}_5\text{O}_2^+$ ) and Eigen ( $\text{H}_9\text{O}_4^+$ ) configurations.<sup>38,56</sup>

In general, we find SCAN yields a substantially fewer number of concerted PTs than PBE0-TS. Taking the PT frequency of hydronium shown in Figs. 7(b) and (d) as an example, the frequency of double jumps from SCAN (12.0) is about half of that from PBE0-TS (22.1); similar conclusion can be drawn for triple jumps and quadruple jumps. The lower number of concerted PT events leads to a relatively lower diffusion coefficient of hydronium from SCAN as compared to those from PBE0-TS. The reason can be analyzed from the molecular structure involved in the double jumps, which involve three water molecules that form a waterwire.<sup>18</sup> The third water molecule most likely comes from the second nearest neighbor of the first water molecule. We plot the radial distribution function  $g_{\text{O}^*\text{O}^w}(\mathbf{r})$  from the two trajectories (SCAN and PBE0-TS) in Fig. 8, where we can see that the first peak of  $g_{\text{O}^*\text{O}^w}$  from PBE0-TS is closer to the central oxygen atom of hydronium as compared to SCAN. This indicates that SCAN gives rise to a slightly more hydrophobic hydronium than PBE0-TS, in consistent with previous analysis. As a result, the hydronium described by PBE0-TS is more likely to donate its protons to its neighboring molecules, resulting in more frequent PT events. Furthermore, the second peak from the SCAN trajectory in Fig. 8 is significantly lower than that of PBE0-TS, suggesting a relatively lower local water density in the second solvation shell of hydronium. The lack of enough water molecules in the second solvation shell of hydronium prevents the protons from jumping two or more times within a burst of PT events. As for the hydroxide ion, since both functionals prefer hyper-coordination structure for the accepted end, frequencies of proton jumps of all types by the two functionals are similarly low. In particular, the frequency of rattling events by SCAN is substantially lower than that by PBE0-TS. The reason may be attributed to the more preferred hyper-coordinated structure of hydroxide from SCAN than PBE0-TS.

We used the Einstein equation to compute the diffusion coefficient of ions as

$$D = \lim_{t \rightarrow \infty} \frac{\|\mathbf{r}(t) - \mathbf{r}(0)\|^2}{6t}, \quad (1)$$

where the mean square displacement (MSD) is defined as  $\|\mathbf{r}(t) - \mathbf{r}(0)\|^2$  with  $\mathbf{r}(t)$  depicts the atom position at time  $t$ . The results are listed in Table I. In order to obtain a reasonable value of  $D$ , we split the trajectories into multiple segments with a length of 12 ps and

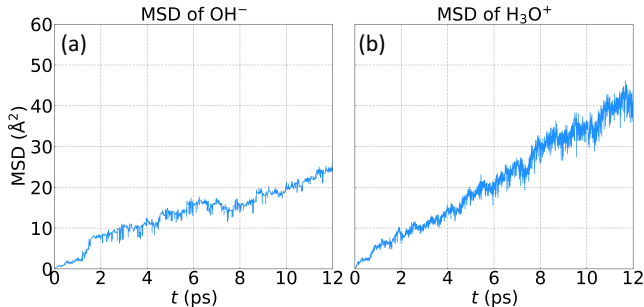


FIG. 9. Mean square displacements (MSD) extracted from the SCAN trajectories of  $\text{OH}^-$ (aq) and  $\text{H}_3\text{O}^+$ (aq) are displayed separately in subplots (a) and (b).

TABLE I. Diffusion coefficients of  $\text{H}_3\text{O}^+$ (aq) and  $\text{OH}^-$ (aq) ( $10^{-9}\text{m}^{-2}/\text{s}$ ). The experimental data<sup>7-9</sup> and PBE0-TS results are compared in Ref. 16 and listed here.

	SCAN	PBE0-TS	Exp. ( $\text{D}_2\text{O}$ )	Exp. ( $\text{H}_2\text{O}$ )
$\text{OH}^-$ (aq)	2.9	3.7	$3.2^7$ , $3.1^9$	$5.4^7$ , $5.2^9$
$\text{H}_3\text{O}^+$ (aq)	5.7	8.3	$6.9^7$ , $6.7^9$	$9.6^7$ , $9.4^9$

the initial snapshots are displaced by an interval of 3 ps. The resulting MSDs of solvated hydroxide and hydronium ions are shown in Figs. 9(a) and (b), respectively. Here we find that the diffusion of hydroxide is substantially slower than hydronium, in consistent with the experimental data and previous analysis. To be specific, the diffusion coefficients of both water ions from SCAN trajectories are relatively smaller than those of PBE0-TS. As listed in Table. I, SCAN (PBE0-TS) predicts  $D$  of hydronium and hydroxide to be  $5.7$  ( $8.3$ )  $\times 10^{-9}\text{m}^2/\text{s}$  and  $2.9$  ( $3.7$ )  $\times 10^{-9}\text{m}^2/\text{s}$ , respectively. Based on previous analysis of the structural, electronic, and dynamic properties of the two ions, we infer that the relatively lower  $D$  values from SCAN originate from the different HB networks described by SCAN and PBE0-TS. In detail, the oxygen site of hydroxide described by SCAN is more hydrophilic and the hydroxide anion is more often solvated by a stable hyper-coordinated structure with four or even five HBs connected with neighboring water molecules. The hyper-coordinated structure turns the ion into an asleep mode and hinders the PT events, preventing itself from fast structural diffusion. As a result, the PT of hydroxide prefers the stepwise motion. On the other hand, the solvated hydronium described by SCAN has a relatively smaller hydrophilicity than PBE0-TS. However, the stable three HBs still form between the protons

of hydronium and neighboring water molecules. In this regard, the concerted PT character is preserved for hydronium. Notably, a lack of the second neighbors further prevents concerted PTs from occurring, which substantially lower the frequency of PT bursts in hydronium. Consequently, the diffusivity of hydronium is lowered as compared to the result from PBE0-TS. In conclusion, the diffusivities of both hydroxide and hydronium ions are lowered from SCAN as compared to those from PBE0-TS, and both functionals predict that hydroxide diffuses slower than hydronium, in consistent with the experiments.

#### IV. CONCLUSIONS

Accurate AIMD simulations of water with ions including hydronium and hydroxide have long been puzzled and hindered due to the lack of suitable XC functionals. We proposed that the general-purpose SCAN XC functional could be an appropriate choice in modeling solvated hydronium and hydroxide ions in liquid water. We performed systematic investigations on the structural, electronic, and dynamical properties of both solvated hydroxide and hydronium ions. Specifically, we studied the amphiphilic properties, the solvation structures, the electronic structures, and the dynamic properties of the two ions. Although the hybrid functional plus van der Waals correction (PBE0-TS) provides a satisfactory picture for the two ions, the computational costs are extremely high. In this regard, we compared the SCAN results to the counterparts from PBE0-TS and the main conclusions are summarized as follows.

The SCAN functional qualitatively reproduces the amphiphilic nature of both water ions as compared to the PBE0-TS functional. In detail, the oxygen site of hydroxide prefers to accept four or even five HBs while donating an unstable H-bond, and SCAN functional predicted substantially more hydroxide ions that accept 5 HBs than PBE0-TS. Meanwhile, hydronium stably donates all of its three protons to neighboring molecules and hardly accepts HBs. Due to the increased number of accepted HBs at the oxygen site of hydroxide, SCAN produces a pot-like solvation structure of hydroxide, which generally agrees well with the result from PBE0-TS and experiment. Note that the different features of the HB network and solvation structure of hydroxide and hydronium origins from their electronic structure. Thus, we analyzed the distributions of MLWF centers, and found the locations of the lone pair and bonding pair electrons respectively determine the hydrophobic and hydrophilic

environments of  $\text{OH}^{-1}(\text{aq})$ ,  $\text{H}_2\text{O}$ , and  $\text{H}_3\text{O}^{+}(\text{aq})$  molecules. Generally, compared to the results from PBE0-TS, we found SCAN yielded a closer distance between the lone pairs and the oxygen atom and a larger distance between the bonding pairs and the protons. As a result, the hydroxide anion from SCAN becomes more hydrophilic on its both ends while the hydronium cation from SCAN becomes slightly more hydrophobic on its two ends. The two competing effects affect the HB network described by SCAN and subsequently determine the dynamic property, particularly for the ubiquitous PT events. On one hand, the hyper-coordinated structure turns the hydroxide into an asleep mode and hinders the PT events; both SCAN and PBE0-TS predict that the PT of hydroxide prefers the stepwise motion. On the other hand, the concerted PT character is preserved for hydronium. However, a lack of the second neighbors further prevents concerted PTs from occurring, significantly lowering the frequency of PT bursts in hydronium. Consequently, the diffusivity of hydronium is lowered as compared to the result from PBE0-TS. In summary, the diffusivities of both hydroxide and hydronium ions are lowered from SCAN as compared to those from PBE0-TS, and both functionals predict that hydroxide diffuses slower than hydronium, in consistent with the experiments.

In conclusion, the SCAN XC functional that adopted in AIMD simulations is already known as an excellent XC functional in describing a variety properties of liquid water. In this work, we further demonstrate that SCAN stands out as the long awaited general-purpose XC functional that can accurately and efficiently predict various properties of solvated hydroxide and hydronium ions in ambient liquid water. In addition, it would be interesting to further consider the nuclear quantum effects in affecting the physical properties of the two ions, which is beyond the scope of this work but can be explored in future. We are looking forward to the usage of SCAN in modeling a variety of important physical and chemical processes that involve hydroxide and hydronium ions.

### **Acknowledgements**

The work of M.C. is supported by the National Science Foundation of China under Grant No. 12074007 and No. 12122401. Parts of the numerical simulations were performed on the High Performance Computing Platform of CAPT. The work by C.Z. and X.W. was supported by National Science Foundation through Award No. DMR-2053195 and No. DMR-1552287. This research used resources of the National Energy Research Scientific Computing Center

(NERSC), which is supported by the U.S. Department of Energy (DOE), Office of Science under Contract No. DE-AC02-05CH11231.

### Availability of Data

The data that support the findings of this study are available from the corresponding author upon reasonable request.

### REFERENCES

- <sup>1</sup>N. Agmon, H. J. Bakker, R. K. Campen, R. H. Henchman, P. Pohl, S. Roke, M. Thämer, and A. Hassanali, *Chemical Reviews* **116**, 7642 (2016).
- <sup>2</sup>de Grotthuss, *Annales de Chimie LVIII* **58**, 54 (1806).
- <sup>3</sup>K.-D. Kreuer, *Chemistry of Materials* **8**, 610 (1996).
- <sup>4</sup>S. Cukierman, *Biochimica et Biophysica Acta (BBA) - Bioenergetics* **1757**, 876 (2006), ISSN 0005-2728, proton Transfer Reactions in Biological Systems.
- <sup>5</sup>C. A. Wraight, *Biochimica et Biophysica Acta (BBA) - Bioenergetics* **1757**, 886 (2006), ISSN 0005-2728, proton Transfer Reactions in Biological Systems.
- <sup>6</sup>B. Halle and G. Karlström, *J. Chem. Soc., Faraday Trans. 2* **79**, 1031 (1983).
- <sup>7</sup>B. Halle and G. Karlström, *J. Chem. Soc., Faraday Trans. 2* **79**, 1047 (1983).
- <sup>8</sup>H. Weingärtner and C. A. Chatzidimitriou-Dreismann, *Nature* **346**, 548 (1990).
- <sup>9</sup>J. H. Sluyters and M. Sluyters-Rehbach, *The Journal of Physical Chemistry B* **114**, 15582 (2010).
- <sup>10</sup>A. Luzar and D. Chandler, *Nature* **379**, 55 (1996).
- <sup>11</sup>D. Marx, M. E. Tuckerman, J. Hutter, and M. Parrinello, *Nature* **397**, 601 (1999).
- <sup>12</sup>P. Hohenberg and W. Kohn, *Phys. Rev.* **136**, 864B (1964).
- <sup>13</sup>W. Kohn and L. J. Sham, *Phys. Rev.* **140**, 1133A (1965).
- <sup>14</sup>M. E. Tuckerman, K. Laasonen, M. Sprik, and M. Parrinello, *Journal of Physics: Condensed Matter* **6**, A93 (1994).
- <sup>15</sup>M. E. Tuckerman, A. Chandra, and D. Marx, *Accounts of Chemical Research* **39**, 151 (2006), pMID: 16489735.
- <sup>16</sup>M. Chen, L. Zheng, B. Santra, H.-Y. Ko, R. A. DiStasio Jr, M. L. Klein, R. Car, and X. Wu, *Nature Chemistry* **10**, 413 (2018).

- <sup>17</sup>A. Hassanali, M. K. Prakash, H. Eshet, and M. Parrinello, Proceedings of the National Academy of Sciences **108**, 20410 (2011), ISSN 0027-8424.
- <sup>18</sup>A. Hassanali, F. Giberti, J. Cuny, T. D. Kühne, and M. Parrinello, Proceedings of the National Academy of Sciences **110**, 13723 (2013), ISSN 0027-8424.
- <sup>19</sup>A. W. Sakti, Y. Nishimura, and H. Nakai, WIREs Computational Molecular Science **10**, e1419 (2020).
- <sup>20</sup>A. P. Gaiduk, F. Gygi, and G. Galli, The Journal of Physical Chemistry Letters **6**, 2902 (2015), pMID: 26267178.
- <sup>21</sup>M. Chen, H.-Y. Ko, R. C. Remsing, M. F. Calegari Andrade, B. Santra, Z. Sun, A. Selloni, R. Car, M. L. Klein, J. P. Perdew, et al., Proceedings of the National Academy of Sciences **114**, 10846 (2017).
- <sup>22</sup>R. A. DiStasio, B. Santra, Z. Li, X. Wu, and R. Car, The Journal of Chemical Physics **141**, 084502 (2014).
- <sup>23</sup>K. Laasonen, F. Csajka, and M. Parrinello, Chemical Physics Letters **194**, 172 (1992), ISSN 0009-2614.
- <sup>24</sup>K. Laasonen, M. Parrinello, R. Car, C. Lee, and D. Vanderbilt, Chemical Physics Letters **207**, 208 (1993).
- <sup>25</sup>M. J. Gillan, D. Alfè, and A. Michaelides, The Journal of Chemical Physics **144**, 130901 (2016).
- <sup>26</sup>J. Schmidt, J. VandeVondele, I. F. W. Kuo, D. Sebastiani, J. I. Siepmann, J. Hutter, and C. J. Mundy, The Journal of Physical Chemistry B **113**, 11959 (2009).
- <sup>27</sup>J. Wang, G. Román-Pérez, J. M. Soler, E. Artacho, and M.-V. Fernández-Serra, The Journal of Chemical Physics **134**, 024516 (2011).
- <sup>28</sup>G. Miceli, S. de Gironcoli, and A. Pasquarello, The Journal of Chemical Physics **142**, 034501 (2015).
- <sup>29</sup>J. P. Perdew, M. Ernzerhof, and K. Burke, J. Chem. Phys. **105**, 9982 (1996).
- <sup>30</sup>C. Adamo and V. Barone, J. Chem. Phys. **110**, 6158 (1999).
- <sup>31</sup>Y.-L. S. Tse, C. Knight, and G. A. Voth, The Journal of Chemical Physics **142**, 014104 (2015).
- <sup>32</sup>K. Burke, J. P. Perdew, and Y. Wang, *Derivation of a Generalized Gradient Approximation: The PW91 Density Functional* (Springer US, Boston, MA, 1998), pp. 81–111.
- <sup>33</sup>A. D. Boese, N. L. Doltsinis, N. C. Handy, and M. Sprik, The Journal of Chemical Physics

- 112**, 1670 (2000).
- <sup>34</sup>A. D. Becke, *Physical Review A* **38**, 3098 (1988).
- <sup>35</sup>C. Lee, W. Yang, and R. G. Parr, *Physical Review B* **37**, 785 (1988).
- <sup>36</sup>M. E. Tuckerman, D. Marx, and M. Parrinello, *Nature* **417**, 925 (2002).
- <sup>37</sup>A. Tkatchenko and M. Scheffler, *Phys. Rev. Lett.* **102**, 073005 (2009).
- <sup>38</sup>D. Marx, *ChemPhysChem* **7**, 1848 (2006).
- <sup>39</sup>A. Botti, F. Bruni, S. Imberti, M. A. Ricci, and A. K. Soper, *The Journal of Chemical Physics* **119**, 5001 (2003).
- <sup>40</sup>H.-Y. Ko, J. Jia, B. Santra, X. Wu, R. Car, and R. A. DiStasio Jr., *Journal of Chemical Theory and Computation* **16**, 3757 (2020).
- <sup>41</sup>P. J. Sun J, Ruzsinszky A, *Phys. Rev. Lett.* **115**, 036402 (2015).
- <sup>42</sup>J. W. Furness, A. D. Kaplan, J. Ning, J. P. Perdew, and J. Sun, *The Journal of Physical Chemistry Letters* **11**, 8208 (2020).
- <sup>43</sup>M. W. Linstrom PJ, *Nist chemistry webbook; nist standard reference database no. 69*, Gaithersburg, MD (2001).
- <sup>44</sup>H. WM, *Crc handbook of chemistry and physics*, Boca Raton, FL (2005).
- <sup>45</sup>J. Sun, R. C. Remsing, Y. Zhang, Z. Sun, A. Ruzsinszky, H. Peng, Z. Yang, A. Paul, U. Waghmare, X. Wu, et al., *Nature Chemistry* **8**, 831 (2016).
- <sup>46</sup>L. Zheng, M. Chen, Z. Sun, H.-Y. Ko, B. Santra, P. Dhuvad, and X. Wu, *The Journal of Chemical Physics* **148**, 164505 (2018).
- <sup>47</sup>J. Xu, M. Chen, C. Zhang, and X. Wu, *Phys. Rev. B* **99**, 205123 (2019).
- <sup>48</sup>K. Sharkas, K. Wagle, B. Santra, S. Akter, R. R. Zope, T. Baruah, K. A. Jackson, J. P. Perdew, and J. E. Peralta, *Proceedings of the National Academy of Sciences* **117**, 11283 (2020), ISSN 0027-8424.
- <sup>49</sup>J. Xu, C. Zhang, L. Zhang, M. Chen, B. Santra, and X. Wu, *Phys. Rev. B* **102**, 214113 (2020).
- <sup>50</sup>R. Car and M. Parrinello, *Phys. Rev. Lett.* **55**, 2471 (1985).
- <sup>51</sup>P. Giannozzi, S. Baroni, N. Bonini, M. Calandra, R. Car, C. Cavazzoni, D. Ceresoli, G. L. Chiarotti, M. Cococcioni, I. Dabo, et al., *J. Phys.: Condens. Matter* **21**, 395502 (2009).
- <sup>52</sup>D. R. Hamann, M. Schlüter, and C. Chiang, *Phys. Rev. Lett.* **43**, 1494 (1979).
- <sup>53</sup>S. Nosé, *J. Chem. Phys.* **81**, 511 (1984).
- <sup>54</sup>W. G. Hoover, *Phys. Rev. A* **31**, 1695 (1985).

<sup>55</sup>G. J. Martyna, M. L. Klein, and M. Tuckerman, *J. Chem. Phys.* **97**, 2635 (1992).

<sup>56</sup>D. Marx, A. Chandra, and M. E. Tuckerman, *Chemical Reviews* **110**, 2174 (2010).